JACS
JOURNAL OF THE AMERICAN CHEMICAL SOCIETY
pubs.acs.org/JACS
Article

Cobalt-Doped Ru@RuO_2 Core−Shell Heterostructure for Efficient Acidic Water Oxidation in Low-Ru-Loading Proton Exchange Membrane Water Electrolyzers

Jinghao Chen,[#] Yirui Ma,[#] Chen Cheng,[#] Tao Huang, Ruihao Luo, Jingwen Xu, Xiaoyang Wang, Taoli Jiang, Hongxu Liu, Shuang Liu, Ting Huang,* Liang Zhang,* and Wei Chen*

Cite This: *J. Am. Chem. Soc.* 2025, 147, 8720−8731

ABSTRACT: Proton exchange membrane water electrolysis (PEMWE) is a highly promising hydrogen production technology for enabling a sustainable energy supply. Herein, we synthesize a single-atom Co-doped core−shell heterostructured Ru@RuO_2 (Co-Ru@RuO_2) catalyst via a combination of ultrafast pulse-heating and calcination methods as an iridium (Ir)-free and durable oxygen evolution reaction (OER) catalyst in acidic conditions. Co-Ru@RuO_2 exhibits a low overpotential of 203 mV and excellent stability over a 400 h durability test at 10 mA cm^{-2}. When implemented in industrial PEMWE devices, a current density of 1 A cm^{-2} is achieved with only 1.58 V under an extremely low catalyst loading of 0.34 mg_{Ru} cm^{-2}, which is decreased by 4 to 6 times as compared to other reported Ru-based catalysts. Even at 500 mA cm^{-2}, the PEMWE device could work stably for more than 200 h. Structural characterizations and density functional theory (DFT) calculations reveal that the single-atom Co doping and the core−shell heterostructure of Ru@RuO_2 modulate the electronic structure of pristine RuO_2, which reduce the energy barriers of OER and improve the stability of surface Ru. This work provides a unique avenue to guide future developments on low-cost PEMWE devices for hydrogen production.

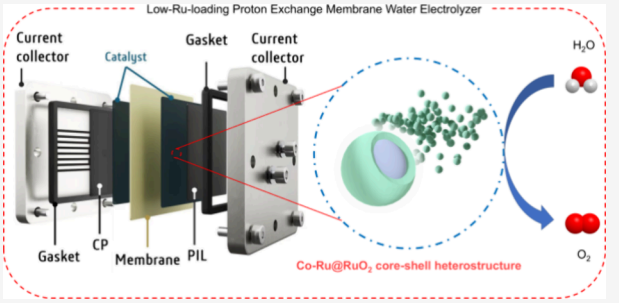

1. INTRODUCTION

The utilization of renewable electricity for water electrolysis is considered a promising and sustainable approach for green hydrogen production.[1,2] Currently, the predominant alkaline water electrolysis (AWE) technology faces several challenges, including product gas crossover, high ohmic resistance, limited current density, and low operating pressure.[3] In comparison to traditional alkaline electrolysis, proton exchange membrane water electrolysis (PEMWE) offers advantages such as faster kinetics, higher operating current density (up to 2−3 A cm^{-2}), and the production of high-purity hydrogen (>99.9999 vol %), which attract broaden research and industrial interests.[4−6] However, the OER at the anode is a four-proton-coupled electron transfer process, and its efficiency is hindered by the higher reaction barrier compared to the hydrogen evolution reaction (HER) in the water-splitting process.[6] Additionally, the harsh acidic and strongly oxidative operating conditions pose significant challenges for the development of high-performance acidic OER electrocatalysts, thereby impeding the widespread application of PEMWE.[7]

For decades, IrO_2- and RuO_2-based materials have been regarded as benchmark electrocatalysts for achieving an optimal balance between stability and activity in acidic OER.[8] However, Ir-based materials face challenges such as low mass activity, extremely low earth abundance, and high cost (US$162,279 kg^{-1}), limiting their practical applications on a large scale. In contrast, Ru (US$16,090 kg^{-1}) presents a more cost-effective option, being 1/10 the cost of Ir, and typically exhibits higher intrinsic activity. This positions Ru-based catalysts as appealing candidates to strike a balance between cost and activity in commercial PEMWE devices. Despite these advantages, the utilization of Ru-based catalysts for acidic OER encounters a major obstacle, which is the poor stability (less than 100 h at 10 mA cm^{-2}) in acidic conditions. This is attributed to the overoxidation of Ru to high-valence Ru^{n+} ($n > 4$) materials, such as soluble RuO_4, in highly oxidative environments.[9,10] This phenomenon inevitably leads to the collapse of the crystal structure, the dissolution of active sites, and subsequent degradation of the catalytic performance.

Carbon, given its widespread natural occurrence, has emerged as a favorable substrate for various catalysts owing to its exceptional conductivity, extensive surface area, and

Received: December 19, 2024
Revised: February 1, 2025
Accepted: February 6, 2025
Published: February 25, 2025

https://doi.org/10.1021/jacs.4c18238
J. Am. Chem. Soc. 2025, 147, 8720−8731

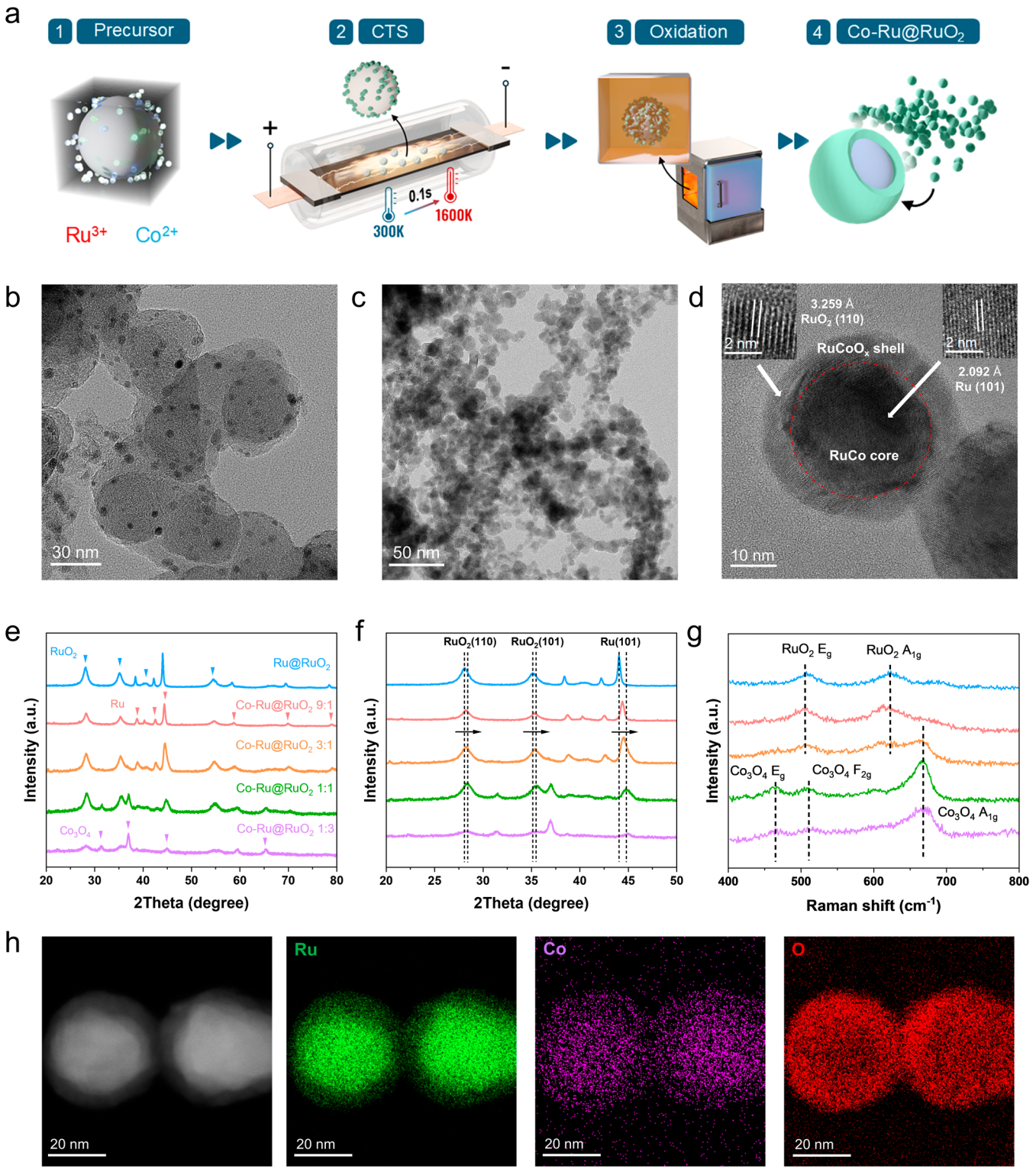

Figure 1. Synthesis and characterization of Co-Ru@$RuO_2$and Ru@RuO_2. (a) Schematic illustrating the synthesis of Co-Ru@RuO_2. TEM images of (b) $Ru_{0.9}Co_{0.1}$/XC-72 and (c) Co-Ru@RuO_2 9:1. (d) HRTEM image of Co-Ru@RuO_2 9:1 nanoparticles with a core−shell heterostructure. (e, f) XRD patterns of Ru@RuO_2 and Co-Ru@RuO_2 with different Ru/Co ratios. (g) Raman spectra of Ru@RuO_2 and Co-Ru@RuO_2 with different Ru/Co ratios. (h) EDS mapping of Co-Ru@RuO_2 9:1.

robust chemical stability under diverse conditions.[11,12] In the initial investigations of acidic OER, a prevalent approach involved either loading the catalyst onto a carbon support,[13,14] such as carbon nanotubes, or encapsulating the catalyst with carbon[15] to enhance its activity and stability in acidic environments. Nevertheless, this practice reflects a misinterpretation in the assessment of acidic OER catalysts' performance at the laboratory scale. In typical three-electrode tests, the stability assessment of the catalysts often relies on chronopotentiometry (CP), with the current density typically

https://doi.org/10.1021/jacs.4c18238
J. Am. Chem. Soc. 2025, 147, 8720−8731

capped at 10 mA cm^{-2}. However, in industrial PEMWE devices, operational current densities generally range from 1 to 2 A cm^{-2}. Under such elevated current densities, carbon is susceptible to oxidation and dissolution, rendering it incapable of maintaining its stability. In recent years, alternative modification approaches for carbon-free Ru-based catalysts, including heteroatomic doping,[16,17] alloying,[18,19] defect engineering,[20] and strain effect,[21] have significantly enhanced the stability of catalysts in acidic conditions. Some of them have also demonstrated commendable activity and stability in industrial PEMWE devices. However, both in industrial applications and in the majority of current research studies, the mass loading of noble metal-based catalysts at the anode is typically around 2−3 mg cm^{-2}.[22−24] This relatively high mass loading substantially escalates the cost associated with hydrogen production in PEMWE.

In this work, we develop a Co-doped Ru@RuO_2 with a core−shell heterostructure as a robust and efficient catalyst for acidic OER in low-Ru-loading PEMWE devices. Although Co-doped RuO_2 catalysts for acidic OER have been studied in earlier works, such as Co-doped RuO_2 nanorods[17] and Ru/RuO_2-Co_3O_4,[25] none of these studies[26,27] have further optimized their performance in PEMWE devices, especially in the case of low catalyst mass loading. Additionally, Co_3O_4 is a highly effective non-noble metal catalyst for acidic OER, which is attributed to its unique spinel crystal structure.[28] One of the reasons for selecting Co as the dopant in our study is to investigate how the Co doping ratio and phase transition (from Co doping to Co_3O_4 formation) influence the performance of the Co-Ru@RuO_2 catalysts. We first employ the ultrafast pulse-heating technology to synthesize ultrafine RuCo alloy nanoparticles supported on commercial carbon substances (Vulcan XC-72R). Subsequently, the RuCo/XC-72R composite is subjected to high-temperature calcination in air to produce the Co-Ru@RuO_2 catalyst. The designed Ru−Co binary oxide exhibits a low overpotential of 203 mV at 10 mA cm^{-2} and enhanced stability exceeding 400 h at 10 mA cm^{-2}, outperforming commercial RuO_2 at the laboratory scale. When implemented in industrial PEMWE devices, a current density of 1 A cm^{-2} is achieved with only 1.58 V under an extremely low catalyst loading of 0.34 mg_{Ru} cm^{-2}, which is only one-fourth to one-sixth of those of the reported Ru-based catalysts. Furthermore, the Co-Ru@RuO_2 catalyst exhibits stable operation at 500 mA cm^{-2} and 1 A cm^{-2} for over 200 and 70 h, respectively, surpassing the stability of previously reported highly active Ru-based electrocatalysts in PEMWE. The structural characterizations including X-ray absorption spectroscopy (XAS), spherical abbreviation-corrected transmission electron microscopy (AC-TEM), X-ray photoelectron spectroscopy (XPS), and Raman spectroscopy are applied to fully understand the enhanced acidic OER activity and stability of the Co-Ru@RuO_2 catalysts. Furthermore, DFT calculations confirm that both single-atom Co doping and the Ru@RuO_2 core−shell heterostructure could modulate the electronic structure of the pristine RuO_2 catalyst, leading to a reduction in the energy barrier associated with the rate-determining step (RDS) in the OER mechanism, which is responsible for the observable enhancement in the OER activity by the catalyst. This work offers new insights into the development of cost-effective and high-performance catalysts for practical PEMWEs.

2. RESULTS AND DISCUSSION

The synthetic process of the $RuCoO_x$ catalyst is schematically shown in Figure 1a. First, commercial Vulcan XC-72R was subjected to a mild oxidation treatment with nitric acid to introduce oxygenated functional groups onto its surface. The resulting abundance of carboxylic groups facilitated the adsorption of Ru^{3+} and Co^{2+}, forming Ru−Co carboxylate complexes on Vulcan XC-72R. Subsequently, these complexes were placed between two closely attached carbon cloths, with the working temperature of the carbon cloths precisely controlled by the input current from a direct-current (DC) power supply. In the course of the electrical pulse heating process (0.1 s on, 1 s off, repeated 10 times), the elevated temperature (up to 1400 K) rapidly reduced the metal ions to metal nanoparticles. These nanoparticles were securely attached to the carbon supports and subsequently rapidly cooled to avoid agglomeration. The morphology of the RuCo/XC-72R (Ru/Co = 9:1) precursor was investigated using TEM. The TEM image revealed a uniform deposition of RuCo nanoparticles onto the carbon black substrates (Figure 1b). Utilizing the ultrafast pulse-heating method, the particle size of RuCo was meticulously controlled to approximately 4 to 5 nm. High-resolution TEM (HRTEM) image of the RuCo nanoparticles is depicted in Figure S1, illustrating lattice fringes with a spacing of approximately 0.205 nm, which corresponds to the (101) plane of the Ru-based catalysts. The slight reduction in lattice fringe spacing for Ru in the RuCo nanoparticles compared to bulk Ru (0.206 nm) is attributed to the incorporation of Co. Second, the acquired RuCo/XC-72R was subjected to annealing in air to facilitate the conversion of RuCo nanoparticles to $RuCoO_x$, concurrently removing the carbon supports. After the air-annealing process, RuCo nanoparticles undergo noticeable oxidation and particle growth, as is evident in the TEM images presented in Figure 1c,d. The oxidized $RuCoO_x$ nanoparticles maintain a uniform size, but their average size increases to approximately 15 nm. The examination of lattice spacing reveals distinct lattice fringes corresponding to the (110) and (101) crystal planes of RuO_2 and Ru, respectively. This observation confirms the core−shell heterostructure of the $RuCoO_x$ nanoparticles. Here, Co-doped RuO_2 catalysts with various doping levels were prepared by controlling the Ru/Co ratio in the precursor solution, specifically 9:1, 3:1, 1:1, and 1:3. According to the TEM results, the synthesized $RuCoO_x$ catalysts are denoted as Co-Ru@RuO_2 (9:1, 3:1, 1:1, and 1:3) based on different Ru/Co feed ratios. The HRTEM images of these Co-Ru@RuO_2 catalysts and the homemade Ru@RuO_2 catalyst are shown in Figures S2. It can be observed that both the Co-Ru@RuO_2 3:1 and Ru@RuO_2 catalysts also exhibit a distinct core−shell heterostructure. However, as the Co doping ratio further increases, the Co_3O_4 phase becomes prominent, and the presence of Ru becomes almost undetectable. The X-ray diffraction (XRD) results are consistent with the TEM observations presented above, as shown in Figure 1e. The XRD patterns with detailed peak annotations are shown in Figure S3. It reveals that as the Co doping ratio increases from 0 to 25%, the crystal structure of the synthesized Co-Ru@RuO_2 catalyst exhibits a mixed phase of Ru (PDF #65-7646) and RuO_2 (PDF #43-1027) without the presence of Co_3O_4. When the Co doping ratio is further increased to 50 or 75%, the intensity of Ru and RuO_2 phase peaks decreases significantly, while that of Co_3O_4 gradually increases. This

https://doi.org/10.1021/jacs.4c18238
J. Am. Chem. Soc. 2025, 147, 8720−8731

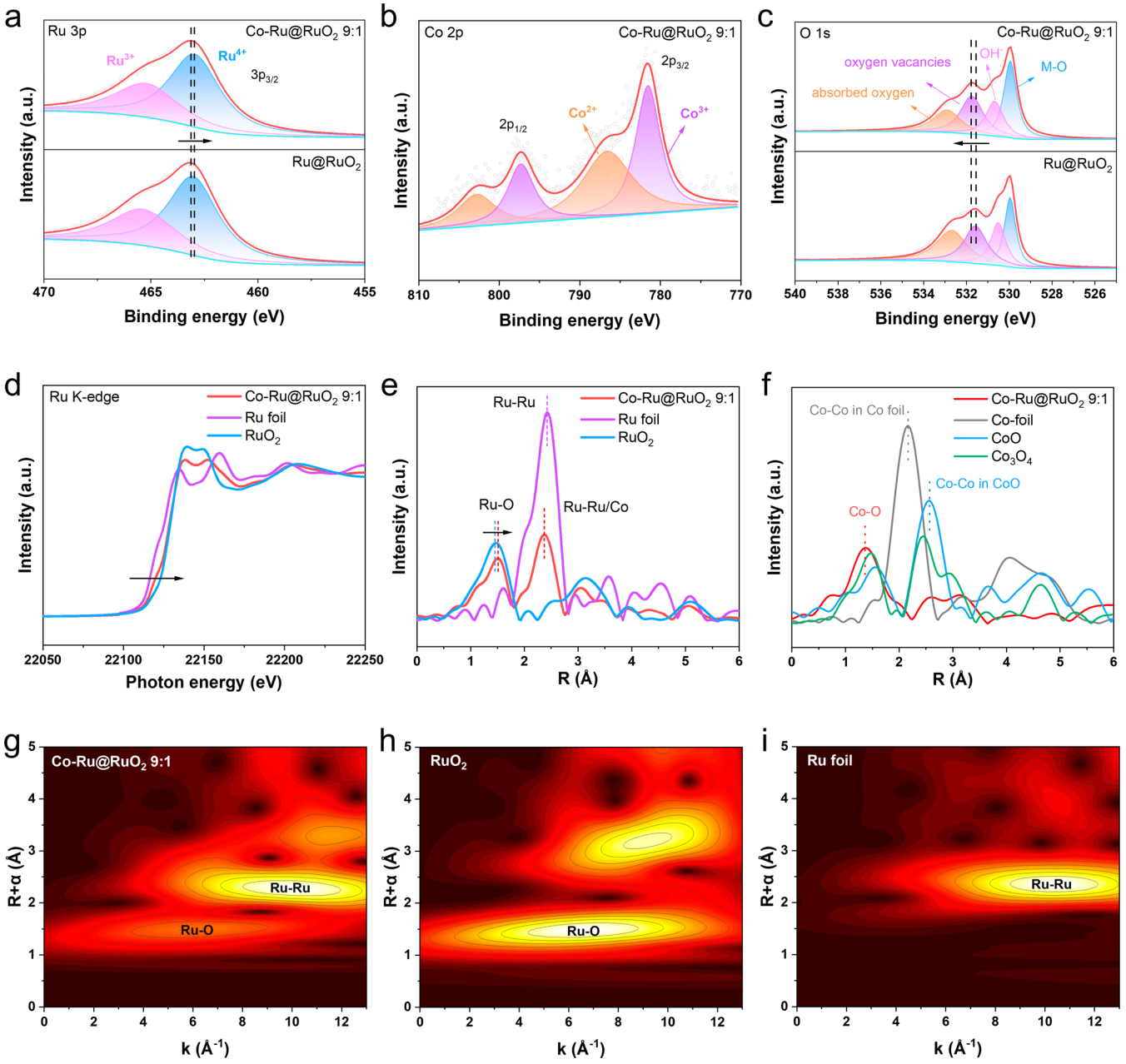

Figure 2. Electronic structure of Co-Ru@RuO_2, Ru@RuO_2, and RuO_2. High-resolution XPS spectra of (a) Ru 3p, (b) Co 2p, and (c) O 1s. Ru K-edge (d) XANES and (e) EXAFS spectra of different samples. (f) Co K-edge EXAFS spectra of different samples. Corresponding WT for (g) Co-Ru@RuO_2, (h) RuO_2, and (i) Ru foil.

also indicates that the appropriate amount of Co doping does not alter the crystal structures of RuO_2 and Ru in the catalyst. Concurrently, as the Co doping ratio increases, noticeable positive shifts in the diffraction peaks of the (110) and (101) planes of RuO_2, as well as the (101) plane of Ru, are observed. This indicates that Co atoms have been successfully incorporated into the Ru@RuO_2 crystal lattice, leading to the formation of a Co-doped Ru@RuO_2 phase with an accompanying lattice shrinkage (Figure 1f). And unless otherwise specified, Co-Ru@RuO_2 in the following text refers to Co-Ru@RuO_2 9:1.

To accurately assess the crystal structure and confirm the absence of Co_3O_4, Raman spectra of Ru@RuO_2 and Co-Ru@RuO_2 with different Ru/Co ratios were recorded (Figure 1g). The lack of a distinct vibration corresponding to Co_3O_4 in Co-Ru@RuO_2 9:1 rules out the formation of Co_3O_4, further confirming the atomic dispersion of Co within the Ru@RuO_2 matrix. However, the vibration peak corresponding to Co_3O_4 A_{1g} is shown in Co-Ru@RuO_2 3:1, 1:1, and 1:3, confirming the presence of the Co_3O_4 phase in these catalysts, which may adversely affect their catalytic performance by covering the catalytic active sites of RuO_2. The successful incorporation of Co and a core−shell heterostructure was also affirmed through energy-dispersive spectroscopic (EDS) elemental mapping of Co-Ru@RuO_2 (Figure 1h), revealing a uniform distribution of Co throughout the entire Ru@RuO_2 matrix. Meanwhile, the EDS results prove that the actual Ru/Co ratio in Co-Ru@RuO_2 9:1 is close to the feed ratio (Figure S4), which is consistent with the results of inductively coupled plasma atomic emission spectrometry (ICP-AES) (Table S1). The air-

https://doi.org/10.1021/jacs.4c18238
J. Am. Chem. Soc. 2025, 147, 8720−8731

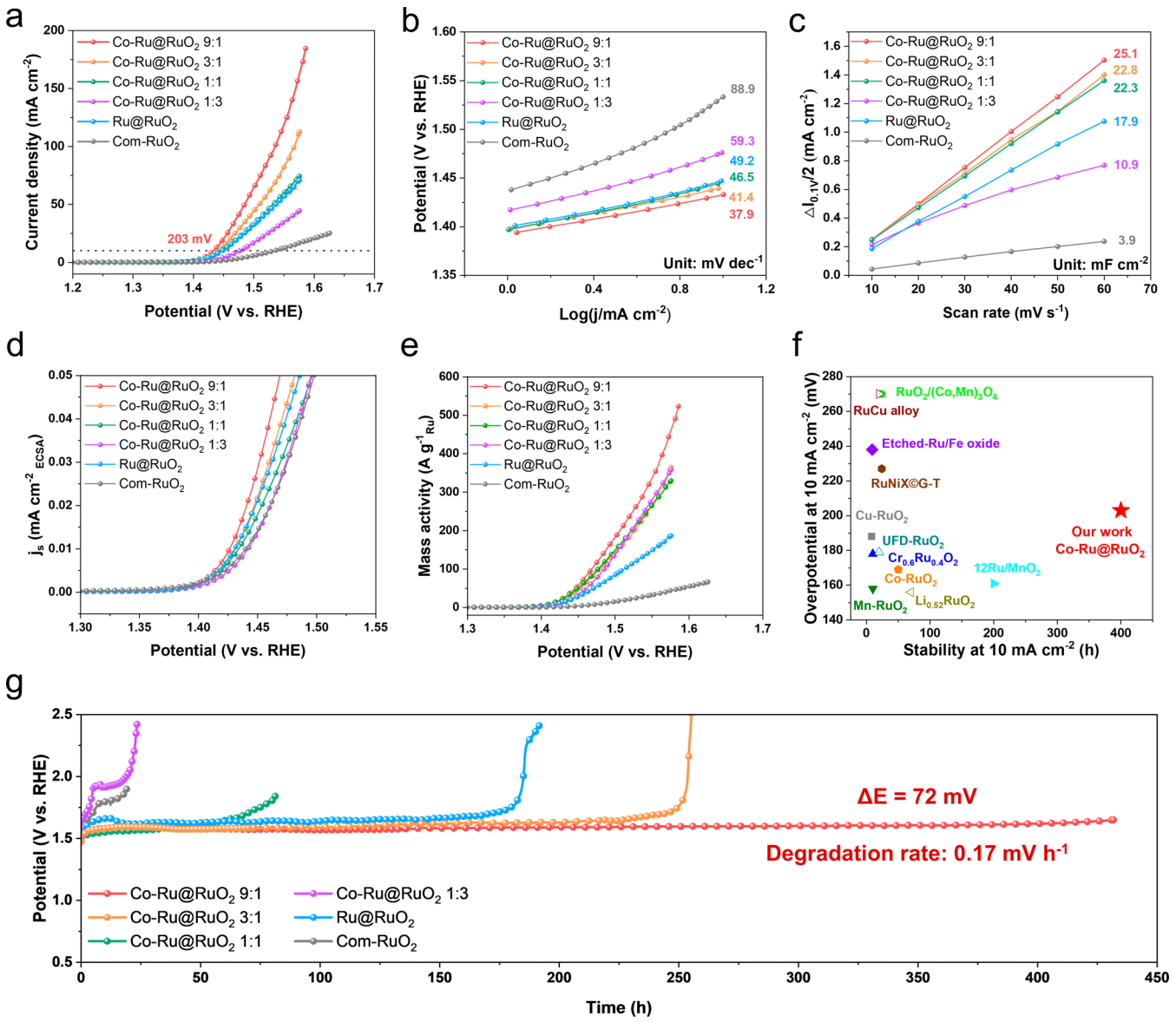

Figure 3. Electrocatalytic OER performance of Co-Ru@RuO_2catalysts. (a) OER polarization curves and (b) Tafel plots of Co-Ru@RuO_2 with different Ru/Co ratios, Ru@RuO_2, and commercial RuO_2. (c) Capacitive current at 0.95 V (vs RHE) against the scan rate and the corresponding C_{dl} values estimated through linear fitting of the plots. (d) ECSA-normalized LSVs and (e) mass activity of Co-Ru@RuO_2 with different Ru/Co ratios, Ru@RuO_2, and commercial RuO_2. (f) The comparison of our work with other work in terms of the overpotential and stability at 10 mA cm^{-2}. (g) Chronopotentiometry test of Co-Ru@RuO_2 with different Ru/Co ratios, Ru@RuO_2, and commercial RuO_2 at 10 mA cm^{-2}.

annealing process significantly enhanced the acidic OER performance (Figure S5), and the optimized air-annealing temperature for the conversion of RuCo nanoparticles to Co-Ru@RuO_2 catalysts was determined to be 500 °C, as illustrated in Figure S6. The Ru/Co precursor molar ratio of 9:1 was established on the basis of a rigorous performance optimization process, which is discussed in the following sections.

To gain a profound understanding of the valence state and distinctive electronic structure of the Co-Ru@RuO_2 electrocatalysts, XPS analysis was conducted on the specimens alongside a comparative sample of Ru@RuO_2. Figure S7 illustrates the high-resolution XPS spectra of Ru 3p, revealing two peaks approximately at the binding energies (BEs) of 462.9 and 465.2 eV corresponding to Ru^{4+} and Ru^{3+} of Ru $3p_{3/2}$, respectively.[16,29] Correspondingly, another two signal peaks of Ru^{4+} and Ru^{3+} appear at 485.1 and 487.1 eV, respectively, attributed to Ru $3p_{1/2}$. Notably, the Ru^{4+} species exhibit a notable negative shift of approximately 0.2 eV compared to Ru@RuO_2 (Figure 2a), indicating a lower valence state of Ru in Co-Ru@RuO_2. Because XPS is only sensitive to several nanometers of the catalyst's surface structure, we can assume that Co doping has lowered the valence state of Ru in the RuO_2 shell. There are four peaks in the high-resolution Co 2p XPS spectrum (Figure 2b): peaks at 781.5 and 797.3 eV are assigned to Co $2p_{3/2}$ and Co $2p_{1/2}$ of Co^{3+}, respectively, and those at 786.6 and 802.8 eV are ascribed to Co $2p_{3/2}$ and Co $2p_{1/2}$ of Co^{2+}, respectively.[30] In high-resolution O 1s XPS spectra (Figure 2c), peaks at 529.9, 530.7, 531.7, and 532.9 eV are identified to be M−O bonds, OH^- groups, oxygen vacancies, and absorbed oxygen, respectively.[31,32] Compared with Ru@RuO_2, the OH^- groups, oxygen vacancies, and absorbed oxygen in Co-Ru@RuO_2 are slightly positively shifted, indicating that O 1s is positively charged.[33] Figures

https://doi.org/10.1021/jacs.4c18238
J. Am. Chem. Soc. 2025, 147, 8720−8731

S8−S10 depict the variation in XPS patterns of Co-Ru@RuO_2 with different Ru/Co ratios. As the doping level of Co increases, the peak shift trend of Ru 3p and 1s mirrors the aforementioned analysis. The positive shift of the O 1s BE and negative shift of the Ru 3p BE provided direct evidences for the weakening of the Ru−O bond covalency by the incorporation of Co into the Ru@RuO_2 matrix. Furthermore, the Co 2p peaks also undergo a negative shift, indicating a slight decrease in the valence state of Co with an increasing Co content. These analyses collectively suggest electron transfer from Ru and Co to O in the Co-Ru@RuO_2 compositions, corroborating electronic interactions among Ru, Co, and O.

Considering that XPS is more sensitive to the surface information on the catalyst, we then performed XAS for both Co-Ru@RuO_2 and commercial RuO_2. As shown in Figure 2d, the absorption edge of the Ru K-edge X-ray absorption near-edge spectroscopy (XANES) for Co-Ru@RuO_2 shifts to a higher energy compared to the Ru foil reference, while slightly shifting to a lower energy than RuO_2. This suggests that the average oxidation state of the Ru species in Co-Ru@RuO_2 is slightly less than +4, which aligns well with the XPS results and the characteristics of the core−shell structure. The corresponding Ru K-edge extended X-ray absorption fine structure (EXAFS) spectrum of Co-Ru@RuO_2 shows two peaks around 1.6 and 2.4 Å, which are assigned to Ru−O and Ru−Ru/Co bonds, respectively[34] (Figure 2e). The elongated Ru−O bonds, compared with RuO_2, confirmed that the Ru−O bond covalency was weakened as a result of Co doping. Three distinct regions are observed in the wavelet transform (WT) of the Ru K-edge EXAFS oscillations of Co-Ru@RuO_2 (Figure 2g), which can be assigned to RuO_2 (Figure 2h) and the Ru foil (Figure 2i), in accordance with the corresponding curves shown in Figure 2e. We also analyzed the Co K-edge XANES (Figure S11) and EXAFS (Figure 2f) spectra of Co-Ru@RuO_2, Co foil, CoO, and Co_3O_4. The Co K-edge XANES spectrum of Co-Ru@RuO_2 shows a higher absorption edge energy than that of the Co foil, indicating the oxidation of Co species. The Co K-edge EXAFS spectra further confirm that the Co atom coordinates with the O atoms at an average Co−O distance of approximately 1.36 Å, which is slightly shorter than the 1.47 and 1.56 Å observed for standard Co_3O_4 and CoO, respectively, due to the intermetallic interactions within the RuO_2 lattice. It is also worth noting that there is no peak at 2.18 Å (Co−Co bond) in Co-Ru@RuO_2 in contrast to the Co foil, demonstrating that Co may exist in the form of single atoms within the Ru@RuO_2 matrix.[30,35,36] To further investigate the presence of Co within the Ru@RuO_2 matrix, we utilized spherical abbreviation-corrected TEM to characterize the Co-Ru@RuO_2 catalyst. The results are shown in Figure S12. The high-angle annular dark-field scanning TEM (HAADF-STEM) images in Figure S12a−c show that Co atoms are dispersed in the RuO_2 matrix. The EDS mappings in Figure S12d also indicate the homogeneous dispersion of Co atoms without any significant aggregation. Combined with the EXAFS results, we can infer that Co exists as single-atom doping within the Ru@RuO_2 matrix. Explicitly, a Ru@RuO_2 core−shell heterostructure has been formed. The above characterizations clearly indicate that single-atom Co dopants were uniformly distributed within the Ru@RuO_2 matrix, where the Ru oxidation states and Ru−O covalency were slightly altered due to the incorporation of Co atoms and the formation of the Ru@RuO_2 core−shell heterostructure.

The catalytic performances of as-prepared Co-Ru@RuO_2 with different Ru/Co ratios toward the OER were directly evaluated on a rotating disc electrode (RDE) set up in 0.5 M H_2SO_4 with platinum and Ag/AgCl as the counter and reference electrode, respectively. For comparison, homemade Ru@RuO_2 and commercial RuO_2 electrocatalysts were also investigated under the same conditions. With the incremental increase in Co-doping from 0 to 50%, the OER performance of the catalysts exhibited a notable enhancement compared to the Ru@RuO_2. However, a further increase in Co doping (to 75%) resulted in a decline in OER activity. The representative Co-Ru@RuO_2 9:1 demonstrated superior OER activity, necessitating only 203 mV overpotential to achieve a current density of 10 mA cm^{-2}. This surpassed the performance of Co-Ru@RuO_2 3:1 (211 mV), Co-Ru@RuO_2 1:1 (216 mV), homemade Ru@RuO_2 (219 mV), Co-Ru@RuO_2 1:3 (247 mV), and commercial RuO_2 (303 mV) samples (Figure 3a). Simultaneously, the Tafel plot (Figure 3b) revealed that the Co-Ru@RuO_2 9:1 catalyst exhibited the smallest Tafel slope of 37.9 mV dec^{-1}, which is lower than that of Co-Ru@RuO_2 3:1 (41.4 mV dec^{-1}), Co-Ru@RuO_2 1:1 (46.5 mV dec^{-1}), homemade Ru@RuO_2 (49.2 mV dec^{-1}), Co-Ru@RuO_2 1:3 (59.3 mV dec^{-1}), and commercial RuO_2 (88.9 mV dec^{-1}). This observation underscores the pivotal role of optimal Co doping in facilitating the kinetics of the OER and accelerating the electron transfer. With the increase of Co doping amount, the Co_3O_4 phase appears in the catalyst, blocking the active sites of RuO_2, which reduces the performance of the catalyst. To compare the intrinsic activity of the prepared Co-Ru@RuO_2 with different Ru/Co ratios, homemade Ru@RuO_2, and commercial RuO_2, the electrochemical specific surface area (ECSA), derived from electrochemical double-layer capacitance (C_{dl}), was employed (Figure 3c and Figure S13). The specific activity (defined as current density normalized by ECSA) of those catalysts was calculated in Figure 3d, which followed the order of Co-Ru@RuO_2 9:1 > Co-Ru@RuO_2 3:1 > homemade Ru@RuO_2 > Co-Ru@RuO_2 1:1 > Co-Ru@RuO_2 1:3 > commercial RuO_2. Furthermore, the TOF value of Co-Ru@RuO_2 9:1 is also superior to that of other control samples (Figure S14). The Co-Ru@RuO_2 9:1 catalyst demonstrated the highest mass activity of 108.4 A g^{-1}_{Ru} at 1.47 V vs RHE (Figure 3e). This value is 1.23, 1.28, 1.59, 2.17, and 13.9 times higher than those of Co-Ru@RuO_2 1:1, Co-Ru@RuO_2 3:1, Co-Ru@RuO_2 1:3, homemade Ru@RuO_2, and commercial RuO_2, respectively. Both the highest specific and mass activities observed for Co-Ru@RuO_2 9:1 among these samples indicate its superior intrinsic activity. Comparisons of the activity and kinetics of Co-Ru@RuO_2 9:1 were also made with respect to recently reported Ru-based catalysts (Figure 3f and Table S2), revealing that the Co-Ru@RuO_2 9:1 catalyst exhibits better activity and faster OER kinetics than most of the Ru-based catalysts in previous reports.

In addition to intrinsic activity, the stability of an electrocatalyst is even more crucial for assessing Ru-based OER electrocatalysts, particularly when aiming for industrial applications. The stability of the synthesized catalysts was first evaluated by a CP test at the current density of 10 mA cm^{-2} on carbon paper. Although our synthesized Ru@RuO_2 showed improved stability compared with Com-RuO_2 (less than 20 h), its performance still degraded at a rapid rate and lasted for no longer than 175 h (Figure 3g). This excellent improvement can be attributed to the formation of core−shell heterostructures. Nevertheless, this performance degradation could be further

https://doi.org/10.1021/jacs.4c18238
J. Am. Chem. Soc. 2025, 147, 8720−8731

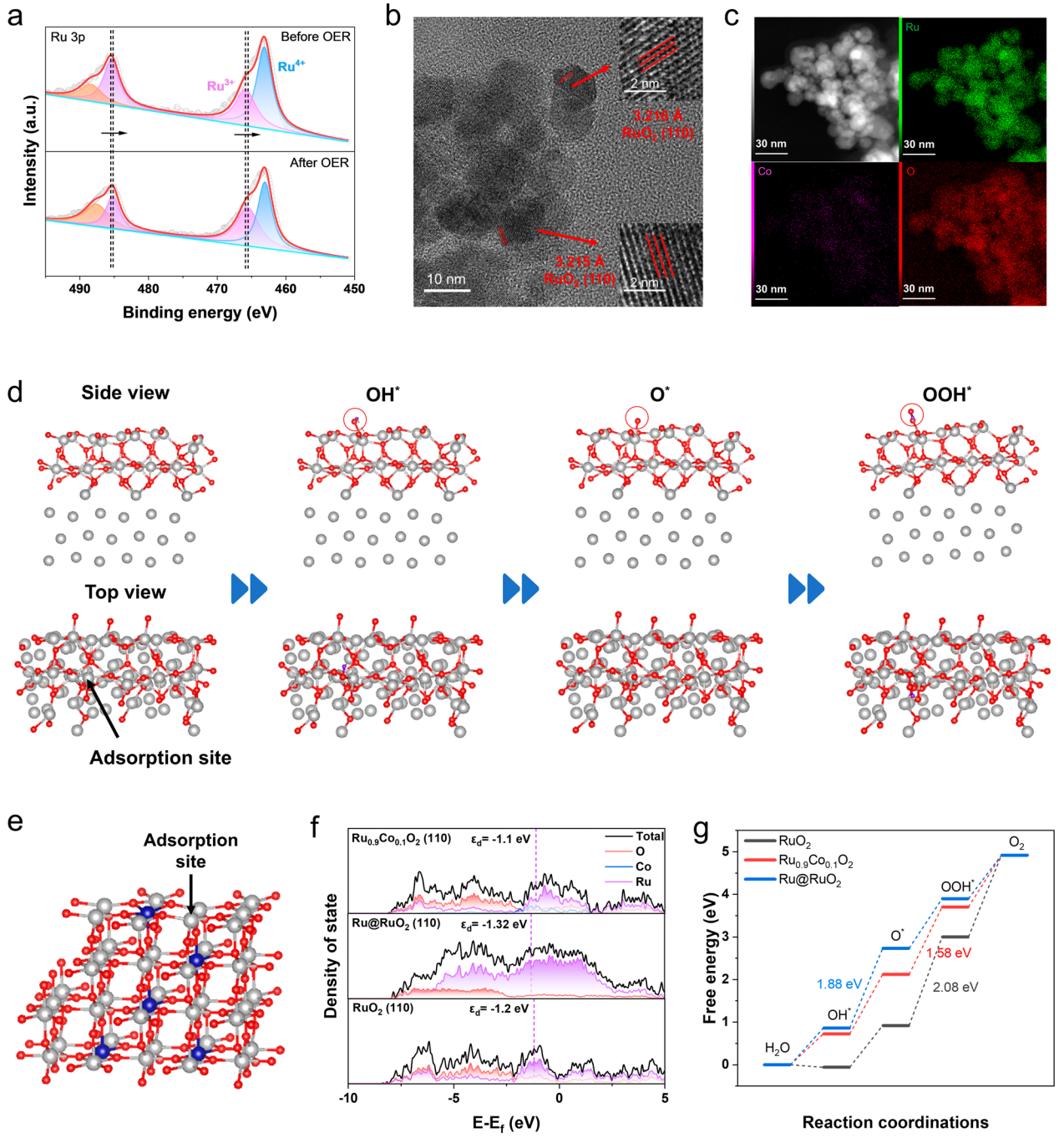

Figure 4. Characterization of Co-Ru@RuO_2 postcycling and DFT calculations. (a) High-resolution Ru 3p XPS spectra of the Co-Ru@RuO_2 catalyst before and after the stability test in acidic media. (b) HRTEM image and (c) EDS mapping of Co-Ru@RuO_2 after the 12 h stability test. (d) OH*, O*, and OOH* intermediates' adsorption configurations on the (110) surface of the Ru@RuO_2 model. The gray, red, and purple balls represent Ru, O, and H atoms, respectively. (e) The model of the Co-doped RuO_2 ($Ru_{0.9}Co_{0.1}O_2$), in which the gray, blue, and red balls represent Ru, Co, and O atoms, respectively. (f) PDOS and (g) Gibbs free energy diagrams of $Ru_{0.9}Co_{0.1}O_2$, Ru@RuO_2, and RuO_2.

mitigated by incorporation of Co. Notably, our Co-Ru@RuO_2 9:1 catalyst exhibited stability for more than 400 h at 10 mA cm^{-2} with a low degradation rate of 0.17 mV h^{-1}, surpassing the endurance of Co-Ru@RuO_2 3:1 (240 h, 0.73 mV h^{-1}), 1:1 (70 h, 2.69 mV h^{-1}), 1:3 (less than 20 h), homemade Ru@RuO_2 (175 h, 0.81 mV h^{-1}), and commercial RuO_2 (less than 20 h) catalysts. Inductively coupled plasma mass spectrometry (ICP-MS) was also utilized to examine the dissolution of active materials during the CP stability test of Co-doped Ru@RuO_2 catalysts (Figure S15). It can be observed that for Co-Ru@RuO_2 9:1, the dissolution of Ru and Co remained at a very low level and varied slightly over time. With the increasing proportion of Co in the catalyst, a significant rise in Co dissolution during the stability tests can be clearly observed, which consequently leads to a decline in the catalyst's stability. And for the Ru@RuO_2 catalyst, the Ru dissolution during stability tests also remains relatively low, providing a partial evidence on the positive role of the core−shell structure in enhancing the stability. These findings suggest that not only can appropriate Co doping enhance the stability of RuO_2 but

https://doi.org/10.1021/jacs.4c18238
J. Am. Chem. Soc. 2025, 147, 8720−8731

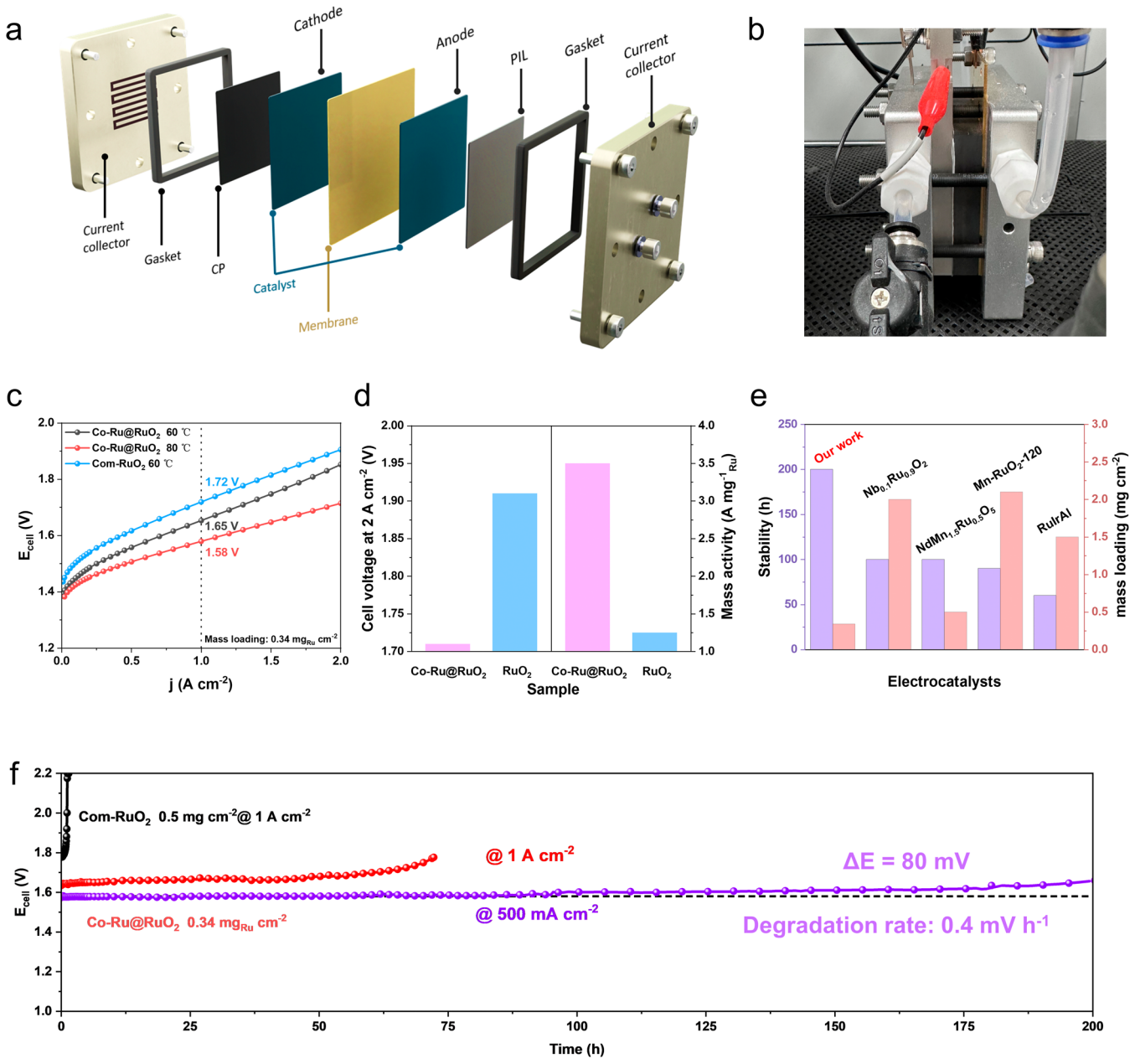

Figure 5. PEMWE tests. (a) Schematic illustration and (b) digital photograph of a single-cell PEMWE. (c) *I*−*V* curves of PEMWE electrolyzers using Co-Ru@RuO_2 as the anodic catalyst without *iR* correction. (d) Cell voltage of the PEMWE to achieve 2 A cm^{-2} (left-hand side panel) and mass activity of the catalysts at 1.6 V (right-hand side panel). (e) Comparison of our work with other works in terms of the stability time and mass loading of the noble metal at PEMWE. (f) Chronopotentiometry testing of the Co-Ru@RuO_2 catalyst at 500 and 1000 mA cm^{-2} and commercial RuO_2 at 1000 mA cm^{-2} in the PEMWE at 60 °C and ambient pressure.

the core−shell heterostructure of Ru@RuO_2 also has a positive impact on the catalyst's performance compared with bare RuO_2. Additionally, the effects of other 3d transition metals as dopants, including Ni and Cr, on the performance of Ru@RuO_2 core−shell heterostructure toward acidic OER were also investigated. The standard RDE tests and stability tests in the three-electrode system confirmed that Co is the optimal dopant (Figure S16).

To gain a deeper understanding on why Co-Ru@RuO_2 exhibits superior inherent OER performance in acidic conditions compared to commercial RuO_2, the Co-Ru@RuO_2 catalyst after the stability test was first characterized. Figure 4a and Figure S17 illustrate the high-resolution Ru 3p and Co 2p XPS patterns of the Co-Ru@RuO_2 catalyst before and after the stability test in acidic media. Notably, the BE for Co in Co-Ru@RuO_2 9:1 after the OER was positively shifted compared to that before the OER, which suggested that Co in Co-Ru@RuO_2 9:1 after the OER was positively charged. However, the BE of Ru 3p in Co-Ru@RuO_2 9:1 after electrolysis presented a slightly lower oxidation state than that before the OER, indicating that the overoxidation of Ru atoms is suppressed due to the single-atom Co doping. Furthermore, the catalyst nanoparticles after the OER were characterized by TEM (Figure S18). HRTEM images (Figure 4b) show that the nanoparticles did not grow significantly and the crystal lattice remained well during the stability test. The EDS mapping

https://doi.org/10.1021/jacs.4c18238
J. Am. Chem. Soc. 2025, 147, 8720−8731

(Figure 4c and Figure S19) also shows that the Co, Ru, and O elements were uniformly distributed in Co-Ru@RuO_2 and the Ru/Co ratio in the nanoparticles was nearly unchanged, which prove the stability of our catalyst. Figure S20 presents a series of in situ Raman spectra for the Co-Ru@RuO_2 catalyst immersed in 0.5 M H_2SO_4 at selected applied potentials versus the Ag/AgCl reference electrode (in saturated KCl). We assign the peaks at 518 and 634 cm^{-1} to RuO_2 E_g and A_{1g} peaks of Co-Ru@RuO_2 and peaks at 980 and 1050 cm^{-1} from SO_4^{2-}.[37] Despite the potential scattering effects from O_2 bubbles diminishing the Raman signal strength, the peaks at 518 and 634 cm^{-1} have almost no change in peak intensity with the increase in the applied potentials, which signify that it maintains an extremely stable structure under positive voltages.

The DFT calculations were also employed to understand the effect of Co dopants and the Ru@RuO_2 core−shell heterostructure on the OER activity. Considering the structure of our Co-Ru@RuO_2 catalyst, to reduce the complexity of the calculations, two models of Co-doped RuO_2 ($Ru_{0.9}Co_{0.1}O_2$) and Ru@RuO_2 were established to illustrate their effects on the OER reaction pathways, as shown in Figure 4d,e. The (110) crystal facet was selected as active surfaces based on the XRD patterns and TEM images for $Ru_{0.9}Co_{0.1}O_2$, Ru@RuO_2 ((101) crystal plane for Ru core), and bare RuO_2. To analyze the excellent OER activity of Co-Ru@RuO_2, the electronic structures of $Ru_{0.9}Co_{0.1}O_2$, Ru@RuO_2, and bare RuO_2 were firstly studied. The projected densities of states (PDOSs) of the active site Ru d orbitals and adsorbed O-p orbitals (Figure 4f) were calculated, which are directly associated with the OER activity. The d-band center (ε_d) with respect to the Fermi level of Ru@RuO_2 is −1.32 eV, while for bare RuO_2, the ε_d is −1.20 eV versus the Fermi level. In other words, the d-band center of Ru in Ru@RuO_2 shifts further from the Fermi level. The adjustment in the d orbitals of Ru leads to a weakened adsorption ability of the catalyst for oxygen atoms, thereby facilitating the formation of *OOH.[13] In addition, the p-band center (ε_p) of O is recognized as an effective descriptor for evaluating OER activity. Typically, a p-band center closer to the Fermi level correlates with improved OER performance.[9] In our calculations, it was found that ε_p shifts from −2.8 eV in RuO_2 to −2.73 eV in $Ru_{0.9}Co_{0.1}O_2$. Besides, the corresponding calculated gaps between ε_d and ε_p for RuO_2, Ru@RuO_2, and $Ru_{0.9}Co_{0.1}O_2$ were 1.6, 1.61, and 1.63 eV, respectively (Table S4). All results indicated that the covalency of Ru−O bonds in $Ru_{0.9}Co_{0.1}O_2$ and Ru@RuO_2 was lower than that of the bare RuO_2, which is in agreement with the XANES results. Generally, weak metal−oxygen covalency can promote the stability of catalysts by suppressing the lattice oxygen mediated mechanism (LOM) pathway during the OER.[38,39] This also proves that Co dopants and the Ru@RuO_2 heterostructure can both regulate the electronic structure of RuO_2 and then affect the adsorption of oxygen intermediates, thus improving the reaction kinetics of the OER.

Based on the above analysis, the traditional adsorption evolution mechanism (AEM) pathway is studied on $Ru_{0.9}Co_{0.1}O_2$, Ru@RuO_2, and bare RuO_2. In an acidic environment (pH = 0), the four-electron OER pathway proceeds through a series of elementary steps. Initially, a water molecule undergoes deprotonation to yield OH* at the catalytically active sites. Subsequently, it deprotonates again to form O* followed by the deprotonation of another water molecule to produce OOH*. Finally, the subsequent deprotonation occurs, leading to the desorption of an O_2 molecule from the surface (Figure 4d). The free energy diagram indicates the activities of $Ru_{0.9}Co_{0.1}O_2$, Ru@RuO_2, and bare RuO_2 on the (110) surface (Figure 4g). Clearly, the formation of OOH* (2.08 eV) was found to be the RDS for the bare RuO_2 surface, which is consistent with previous reports.[40] In contrast, for $Ru_{0.9}Co_{0.1}O_2$ and Ru@RuO_2, the ΔG of their RDS are 1.58 and 1.88 eV, representing reduced energies of 0.5 and 0.2 eV, respectively. This reduction signifies the enhanced intrinsic OER activity of the catalyst due to Co doping and the Ru@RuO_2 heterostructure, which further confirms the results of PDOS analysis and agrees well with the results of electrochemical tests. Regarding stability, we evaluated the energy change associated with the demetalation of surface Ru atoms from the (110) surface of both RuO_2 and $Ru_{0.9}Co_{0.1}O_1$, as the delamination of surface Ru atoms is a potential factor contributing to the low stability of catalysts.[41] The proposed demetalation process of surface Ru is illustrated in Figures S21 and S22. We observed that with the incorporation of Co into the RuO_2 matrix, the energy barrier for Ru demetalation increased from 11.46 to 13.76 eV (Figure S23), suggesting more stable surface Ru atoms in $Ru_{0.9}Co_{0.1}O_2$ than in RuO_2.

Having the excellent performance of Co-Ru@RuO_2 in the three-electrode tests, its activity and stability in the PEMWE device were further evaluated. In this setup, the Co-Ru@RuO_2 catalyst was utilized as the anode catalyst for the OER, while commercial Pt/C (20%) was employed as the cathode catalyst for the HER. A proton exchange membrane (Nafion 115) was interposed between the two catalysts, as shown in Figure 5a,b. The selection of Pt/C for the cathode catalyst was driven by its established characteristics of high HER activity and durability. In the context of hydrogen production in industrial PEM devices, the typical mass loading of anode catalysts, such as RuO_2 or IrO_2, is around 2 to 3 mg cm^{-2}. Even in the state-of-the-art research on Ru-based catalysts, the mass loading typically exceeds 1 mg_{Ru} cm^{-2}.[23,42] Nevertheless, in this study, we achieved remarkable performance even with a much-reduced mass loading of the Co-Ru@RuO_2 catalyst, set at 0.5 mg cm^{-2} (0.34 mg_{Ru} cm^{-2}). The current−voltage characteristic (I−V) curves (without iR correction) in Figure 5c clearly show that under the same mass loading conditions, commercial RuO_2 requires a voltage of 1.72 V to achieve a current density of 1 A cm^{-2} at 80 °C. In contrast, our Co-Ru@RuO_2 catalyst only requires 1.65 and 1.58 V at 60 and 80 °C, respectively, to reach the same current density of 1 A cm^{-2}. The catalyst's activity is among the highest reported for Ru-based catalysts despite its mass loading being only one-fourth to one-sixth of the reported values. Moreover, the voltages (Figure 5d, left panel) required for Co-Ru@RuO_2 and commercial RuO_2 to reach a current density of 2 A cm^{-2} were 1.715 and 1.905 V, respectively. And the mass activity (Figure 5d, right panel) of Co-Ru@RuO_2 at 1.6 V is 3.5 A mg_{Ru}^{-1}, which is approximately 2.8 times higher than that of the commercial RuO_2 (1.25 A mg_{Ru}^{-1}). Additionally, the PEM electrolyzer incorporating Co-Ru@RuO_2 as the anode catalyst consistently maintains a voltage close to 1.6 V during a 200 h continual operation at a current density of 500 mA cm^{-2} with a low degradation rate of 0.4 mV h^{-1}, as depicted in Figure 5f. Even at a current density of 1 A cm^{-2}, our catalyst demonstrates stable operation for more than 70 h. In contrast, at the same low noble metal mass loading, commercial RuO_2 can only work for less than 1 h at the current density of 1 A cm^{-2}. It is noteworthy that in comparison to previously reported electrocatalysts utilized in

https://doi.org/10.1021/jacs.4c18238
J. Am. Chem. Soc. 2025, 147, 8720−8731

PEM electrolyzers, the Co-Ru@RuO_2 catalyst with extremely low noble metal mass loading exhibits excellent intrinsic activity and stability under high current densities that rank among the best performances reported to date (Figure 5e and Table S3). Moreover, we also performed XPS tests on the membrane electrode assembly (MEA) following a stability test conducted at 500 mA cm^{-2} in PEMWE, with the results presented in Figure S24. After prolonged operation of the PEMWE tests, a significant dissolution of Co from the MEA surface was observed. However, the results of the Ru 3p spectra indicated that the structural stability of Ru was well preserved. Additionally, the shift of XPS peaks toward lower binding energies further confirmed that the overoxidation of Ru was effectively suppressed, which aligns with the characterization results obtained for the catalyst after stability tests in the three-electrode system. These findings highlight the dual contributions of Co doping and the core−shell structure in enhancing both the stability and performance of the catalyst under challenging acidic OER and PEMWE conditions.

3. CONCLUSIONS

In summary, we have developed a two-step strategy by combining the rapid pulse-heating and calcination methods to construct single-atom Co doped core−shell heterostructured Ru@RuO_2 as a highly active and stable catalyst toward acidic OER. The Co-Ru@RuO_2 9:1 catalyst demonstrated both higher activity and stability than the other investigated samples. The overpotential is as small as 203 mV to achieve a current density of 10 mA cm^{-2} with stability for 400 h. Furthermore, a PEMWE device fabricated with Co-Ru@RuO_2 as an anode catalyst in an ultralow Ru mass loading of 0.34 mg cm^{-2} can afford a cell voltage of 1.58 V at 1 A cm^{-2} as well as long-term stability over 200 h under 500 mA cm^{-2}. Experimental evidence and DFT calculations unveiled the critical role of single-atom Co dopant and the Ru@RuO_2 core-shell heterostructure, which affected the adsorption of oxygen intermediates and weakened the covalency of Ru−O bonds, thus improving the reaction kinetics and stability of the OER. This work provides a durable solution for the deployment of an Ir-free Ru-based catalyst in low-Ru-loading PEMWE.

■ ASSOCIATED CONTENT

Supporting Information

The Supporting Information is available free of charge at https://pubs.acs.org/doi/10.1021/jacs.4c18238.

Materials, synthetic methods, characterization, electrochemical performance tests, calculation details, and PEMWE tests (PDF)

■ AUTHOR INFORMATION

Corresponding Authors

Ting Huang − *Department of Applied Chemistry School of Chemistry and Materials Science Hefei National Research Center for Physical Sciences at the Microscale, University of Science and Technology of China, Hefei, Anhui 230026, China*; Email: tinghuang@ustc.edu.cn

Liang Zhang − *Institute of Functional Nano and Soft Materials (FUNSOM) Jiangsu Key Laboratory of Advanced Negative Carbon Technologies, Soochow University, Suzhou, Jiangsu 215123, China*; orcid.org/0000-0002-3446-3172; Email: liangzhang2019@suda.edu.cn

Wei Chen − *Department of Applied Chemistry School of Chemistry and Materials Science Hefei National Research Center for Physical Sciences at the Microscale, University of Science and Technology of China, Hefei, Anhui 230026, China*; orcid.org/0000-0002-8018-4529; Email: weichen1@ustc.edu.cn

Authors

Jinghao Chen − *Department of Applied Chemistry School of Chemistry and Materials Science Hefei National Research Center for Physical Sciences at the Microscale, University of Science and Technology of China, Hefei, Anhui 230026, China*

Yirui Ma − *Department of Applied Chemistry School of Chemistry and Materials Science Hefei National Research Center for Physical Sciences at the Microscale, University of Science and Technology of China, Hefei, Anhui 230026, China*

Chen Cheng − *Institute of Functional Nano and Soft Materials (FUNSOM) Jiangsu Key Laboratory of Advanced Negative Carbon Technologies, Soochow University, Suzhou, Jiangsu 215123, China*

Tao Huang − *Department of Applied Chemistry School of Chemistry and Materials Science Hefei National Research Center for Physical Sciences at the Microscale, University of Science and Technology of China, Hefei, Anhui 230026, China*

Ruihao Luo − *Department of Applied Chemistry School of Chemistry and Materials Science Hefei National Research Center for Physical Sciences at the Microscale, University of Science and Technology of China, Hefei, Anhui 230026, China*

Jingwen Xu − *Department of Applied Chemistry School of Chemistry and Materials Science Hefei National Research Center for Physical Sciences at the Microscale, University of Science and Technology of China, Hefei, Anhui 230026, China*

Xiaoyang Wang − *Department of Applied Chemistry School of Chemistry and Materials Science Hefei National Research Center for Physical Sciences at the Microscale, University of Science and Technology of China, Hefei, Anhui 230026, China*

Taoli Jiang − *Department of Applied Chemistry School of Chemistry and Materials Science Hefei National Research Center for Physical Sciences at the Microscale, University of Science and Technology of China, Hefei, Anhui 230026, China*

Hongxu Liu − *Department of Applied Chemistry School of Chemistry and Materials Science Hefei National Research Center for Physical Sciences at the Microscale, University of Science and Technology of China, Hefei, Anhui 230026, China*

Shuang Liu − *Department of Applied Chemistry School of Chemistry and Materials Science Hefei National Research Center for Physical Sciences at the Microscale, University of Science and Technology of China, Hefei, Anhui 230026, China*

Complete contact information is available at: https://pubs.acs.org/10.1021/jacs.4c18238

Author Contributions

#J.C., Y.M., and C.C. contributed equally to this work.

Notes

The authors declare no competing financial interest.

■ ACKNOWLEDGMENTS

W.C. acknowledges the National Natural Science Foundation of China (92372122, 52471242), the Fundamental Research Funds for the Central Universities (WK2060000040, KY2060000150, GG2060127001) and Joint Laboratory for USTC and Yanchang Petroleum (2022ZKD-03). T.H. acknowledges the Anhui Development and Reform Commission (AHZDCYCX-LSDT2023-07) and the National Natural Science Foundation of China (22175163). The authors thank the USTC Supercomputing Center and the USTC Center for Micro and Nanoscale Research and Fabrication. The authors thank BL11B of Shanghai Synchrotron Radiation Facility. This study was partially carried out at the Instrument Center for Physical Science, USTC.

■ REFERENCES

(1) Turner, J. A. Sustainable Hydrogen Production. *Science* **2004**, *305* (5686), 972−974.
(2) Nong, H. N.; Falling, L. J.; Bergmann, A.; Klingenhof, M.; Tran, H. P.; Spöri, C.; Mom, R.; Timoshenko, J.; Zichittella, G.; Knop-Gericke, A.; Piccinin, S.; Pérez-Ramírez, J.; Cuenya, B. R.; Schlögl, R.; Strasser, P.; Teschner, D.; Jones, T. E. Key role of chemistry versus bias in electrocatalytic oxygen evolution. *Nature* **2020**, *587* (7834), 408−413.
(3) Carmo, M.; Fritz, D. L.; Mergel, J.; Stolten, D. A comprehensive review on PEM water electrolysis. *Int. J. Hydrogen. Energy.* **2013**, *38* (12), 4901−4934.
(4) Wu, Z.-Y.; Chen, F.-Y.; Li, B.; Yu, S.-W.; Finfrock, Y. Z.; Meira, D. M.; Yan, Q.-Q.; Zhu, P.; Chen, M.-X.; Song, T.-W.; Yin, Z.; Liang, H.-W.; Zhang, S.; Wang, G.; Wang, H. Non-iridium-based electrocatalyst for durable acidic oxygen evolution reaction in proton exchange membrane water electrolysis. *Nat. Mater.* **2023**, *22* (1), 100−108.
(5) An, L.; Wei, C.; Lu, M.; Liu, H.; Chen, Y.; Scherer, G. G.; Fisher, A. C.; Xi, P.; Xu, Z. J.; Yan, C.-H. Recent Development of Oxygen Evolution Electrocatalysts in Acidic Environment. *Adv. Mater.* **2021**, *33* (20), No. 2006328.
(6) Spöri, C.; Kwan, J. T. H.; Bonakdarpour, A.; Wilkinson, D. P.; Strasser, P. The Stability Challenges of Oxygen Evolving Catalysts: Towards a Common Fundamental Understanding and Mitigation of Catalyst Degradation. *Angew. Chem., Int. Ed.* **2017**, *56* (22), 5994−6021.
(7) Du, K.; Zhang, L.; Shan, J.; Guo, J.; Mao, J.; Yang, C.-C.; Wang, C.-H.; Hu, Z.; Ling, T. Interface engineering breaks both stability and activity limits of RuO_2 for sustainable water oxidation. *Nat. Commun.* **2022**, *13* (1), 5448.
(8) Lin, Y.; Dong, Y.; Wang, X.; Chen, L. Electrocatalysts for the Oxygen Evolution Reaction in Acidic Media. *Adv. Mater.* **2023**, *35* (22), No. 2210565.
(9) Lin, Y.; Tian, Z.; Zhang, L.; Ma, J.; Jiang, Z.; Deibert, B. J.; Ge, R.; Chen, L. Chromium-ruthenium oxide solid solution electrocatalyst for highly efficient oxygen evolution reaction in acidic media. *Nat. Commun.* **2019**, *10* (1), 162.
(10) Yao, Y.; Hu, S.; Chen, W.; Huang, Z.-Q.; Wei, W.; Yao, T.; Liu, R.; Zang, K.; Wang, X.; Wu, G.; Yuan, W.; Yuan, T.; Zhu, B.; Liu, W.; Li, Z.; He, D.; Xue, Z.; Wang, Y.; Zheng, X.; Dong, J.; Chang, C.-R.; Chen, Y.; Hong, X.; Luo, J.; Wei, S.; Li, W.-X.; Strasser, P.; Wu, Y.; Li, Y. Engineering the electronic structure of single atom Ru sites via compressive strain boosts acidic water oxidation electrocatalysis. *Nat. Catal.* **2019**, *2* (4), 304−313.
(11) Su, J.; Musgrave, C. B.; Song, Y.; Huang, L.; Liu, Y.; Li, G.; Xin, Y.; Xiong, P.; Li, M. M.-J.; Wu, H.; Zhu, M.; Chen, H. M.; Zhang, J.; Shen, H.; Tang, B. Z.; Robert, M.; Goddard, W. A.; Ye, R. Strain enhances the activity of molecular electrocatalysts via carbon nanotube supports. *Nat. Catal.* **2023**, *6* (9), 818−828.
(12) Wang, J.; Kong, H.; Zhang, J.; Hao, Y.; Shao, Z.; Ciucci, F. Carbon-based electrocatalysts for sustainable energy applications. *Prog. Mater. Sci.* **2021**, *116*, No. 100717.
(13) Niu, S.; Kong, X.-P.; Li, S.; Zhang, Y.; Wu, J.; Zhao, W.; Xu, P. Low Ru loading $RuO_2/(Co,Mn)_3O_4$ nanocomposite with modulated electronic structure for efficient oxygen evolution reaction in acid. *Applied Catalysis B: Environmental* **2021**, *297*, No. 120442.
(14) Wang, Y.; Lei, X.; Zhang, B.; Bai, B.; Das, P.; Azam, T.; Xiao, J.; Wu, Z.-S. Breaking the Ru−O−Ru Symmetry of a RuO_2 Catalyst for Sustainable Acidic Water Oxidation. *Angew. Chem., Int. Ed.* **2024**, *63* (3), No. e202316903.
(15) Yan, H.; Jiang, Z.; Deng, B.; Wang, Y.; Jiang, Z.-J. Ultrathin Carbon Coating and Defect Engineering Promote RuO_2 as an Efficient Catalyst for Acidic Oxygen Evolution Reaction with Super-High Durability. *Adv. Energy Mater.* **2023**, *13* (23), No. 2300152.
(16) Chen, S.; Huang, H.; Jiang, P.; Yang, K.; Diao, J.; Gong, S.; Liu, S.; Huang, M.; Wang, H.; Chen, Q. Mn-Doped RuO_2 Nanocrystals as Highly Active Electrocatalysts for Enhanced Oxygen Evolution in Acidic Media. *ACS Catal.* **2020**, *10* (2), 1152−1160.
(17) Tian, Y.; Wang, S.; Velasco, E.; Yang, Y.; Cao, L.; Zhang, L.; Li, X.; Lin, Y.; Zhang, Q.; Chen, L. A Co-Doped Nanorod-like RuO_2 Electrocatalyst with Abundant Oxygen Vacancies for Acidic Water Oxidation. *iScience* **2020**, *23* (1), No. 100756.
(18) An, L.; Yang, F.; Fu, C.; Cai, X.; Shen, S.; Xia, G.; Li, J.; Du, Y.; Luo, L.; Zhang, J. A Functionally Stable RuMn Electrocatalyst for Oxygen Evolution Reaction in Acid. *Adv. Funct. Mater.* **2022**, *32* (27), No. 2200131.
(19) Yao, Q.; Huang, B.; Zhang, N.; Sun, M.; Shao, Q.; Huang, X. Channel-Rich RuCu Nanosheets for pH-Universal Overall Water Splitting Electrocatalysis. *Angew. Chem., Int. Ed.* **2019**, *58* (39), 13983−13988.
(20) Zhang, D.; Li, M.; Yong, X.; Song, H.; Waterhouse, G. I. N.; Yi, Y.; Xue, B.; Zhang, D.; Liu, B.; Lu, S. Construction of Zn-doped RuO_2 nanowires for efficient and stable water oxidation in acidic media. *Nat. Commun.* **2023**, *14* (1), 2517.
(21) Qin, Y.; Yu, T.; Deng, S.; Zhou, X.-Y.; Lin, D.; Zhang, Q.; Jin, Z.; Zhang, D.; He, Y.-B.; Qiu, H.-J.; He, L.; Kang, F.; Li, K.; Zhang, T.-Y. RuO_2 electronic structure and lattice strain dual engineering for enhanced acidic oxygen evolution reaction performance. *Nat. Commun.* **2022**, *13* (1), 3784.
(22) Liu, H.; Zhang, Z.; Fang, J.; Li, M.; Sendeku, M. G.; Wang, X.; Wu, H.; Li, Y.; Ge, J.; Zhuang, Z.; Zhou, D.; Kuang, Y.; Sun, X. Eliminating over-oxidation of ruthenium oxides by niobium for highly stable electrocatalytic oxygen evolution in acidic media. *Joule* **2023**, *7* (3), 558−573.
(23) Shi, Z.; Li, J.; Wang, Y.; Liu, S.; Zhu, J.; Yang, J.; Wang, X.; Ni, J.; Jiang, Z.; Zhang, L.; Wang, Y.; Liu, C.; Xing, W.; Ge, J. Customized reaction route for ruthenium oxide towards stabilized water oxidation in high-performance PEM electrolyzers. *Nat. Commun.* **2023**, *14* (1), 843.
(24) Hu, C.; Yue, K.; Han, J.; Liu, X.; Liu, L.; Liu, Q.; Kong, Q.; Pao, C. W.; Hu, Z.; Suenaga, K.; Su, D.; Zhang, Q.; Wang, X.; Tan, Y.; Huang, X. Misoriented high-entropy iridium ruthenium oxide for acidic water splitting. *Sci. Adv.* **2023**, *9* (37), No. eadf9144.
(25) Wang, T.; Li, Z.; Jang, H.; Kim, M. G.; Qin, Q.; Liu, X. Interface Engineering of Oxygen Vacancy-Enriched $Ru/RuO_2-Co_3O_4$ Heterojunction for Efficient Oxygen Evolution Reaction in Acidic Media. *ACS Sustainable Chem. Eng.* **2023**, *11* (13), 5155−5163.
(26) Gong, R.; Liu, B.; Wang, X.; Du, S.; Xie, Y.; Jia, W.; Bian, X.; Chen, Z.; Ren, Z. Electronic Structure Modulation Induced by Cobalt-doping and Lattice-Contracting on Armor-Like Ruthenium Oxide Drives pH-Universal Oxygen Evolution. *Small* **2023**, *19* (4), No. 2204889.
(27) Zhu, W.; Yao, F.; Cheng, K.; Zhao, M.; Yang, C.-J.; Dong, C.-L.; Hong, Q.; Jiang, Q.; Wang, Z.; Liang, H. Direct Dioxygen Radical Coupling Driven by Octahedral Ruthenium−Oxygen−Cobalt Col-

https://doi.org/10.1021/jacs.4c18238
J. Am. Chem. Soc. 2025, 147, 8720−8731

laborative Coordination for Acidic Oxygen Evolution Reaction. *J. Am. Chem. Soc.* **2023**, *145* (32), 17995−18006.
(28) Rong, C.; Wang, S.; Shen, X.; Jia, C.; Sun, Q.; Zhang, Q.; Zhao, C. Defect-balanced active and stable Co_3O_{4-x} for proton exchange membrane water electrolysis at ampere-level current density. *Energy Environ. Sci.* **2024**, *17* (12), 4196−4204.
(29) Li, W.; Zhao, Y.; Liu, Y.; Sun, M.; Waterhouse, G. I. N.; Huang, B.; Zhang, K.; Zhang, T.; Lu, S. Exploiting Ru-Induced Lattice Strain in CoRu Nanoalloys for Robust Bifunctional Hydrogen Production. *Angew. Chem., Int. Ed.* **2021**, *60* (6), 3290−3298.
(30) Ma, X.; Liu, M.; Li, Q.; Xiao, X.; Liu, J.; Xu, X.; Yin, Y.; Qiao, P.; Zhang, L.; Zou, X.; Wang, R.; Jiang, B. Associating Co single atoms with RuO_2 nanoparticles anchor on nitrogen-doped ultrathin porous carbon nanosheets as effective bifunctional oxygen electrocatalysts for rechargeable Zn−air batteries. *J. Mater. Chem. A* **2023**, *11* (31), 16889−16899.
(31) Zhang, L.; Jang, H.; Liu, H.; Kim, M. G.; Yang, D.; Liu, S.; Liu, X.; Cho, J. Sodium-Decorated Amorphous/Crystalline RuO_2 with Rich Oxygen Vacancies: A Robust pH-Universal Oxygen Evolution Electrocatalyst. *Angew. Chem., Int. Ed.* **2021**, *60* (34), 18821−18829.
(32) Chen, S.; Wang, C.; Gao, F.; Yang, Y.; Huang, M.; Tong, H.; Cheng, Z.; Wang, P.; Wang, P.; Tu, J.; Zeng, X.; Chen, Q. An indium-induced-synthesis $In_{0.17}Ru_{0.83}O_2$ nanoribbon as highly active electrocatalyst for oxygen evolution in acidic media at high current densities above 400 mA cm^{-2}. *J. Mater. Chem. A* **2022**, *10* (7), 3722−3731.
(33) Shan, J.; Ling, T.; Davey, K.; Zheng, Y.; Qiao, S.-Z. Transition-Metal-Doped RuIr Bifunctional Nanocrystals for Overall Water Splitting in Acidic Environments. *Adv. Mater.* **2019**, *31* (17), No. 1900510.
(34) Li, Y.; Wang, W.; Cheng, M.; Feng, Y.; Han, X.; Qian, Q.; Zhu, Y.; Zhang, G. Arming Ru with Oxygen-Vacancy-Enriched RuO_2 Sub-Nanometer Skin Activates Superior Bifunctionality for pH-Universal Overall Water Splitting. *Adv. Mater.* **2023**, *35* (24), No. 2206351.
(35) Chen, Y.; Li, X.-Y.; Chen, Z.; Ozden, A.; Huang, J. E.; Ou, P.; Dong, J.; Zhang, J.; Tian, C.; Lee, B.-H.; Wang, X.; Liu, S.; Qu, Q.; Wang, S.; Xu, Y.; Miao, R. K.; Zhao, Y.; Liu, Y.; Qiu, C.; Abed, J.; Liu, H.; Shin, H.; Wang, D.; Li, Y.; Sinton, D.; Sargent, E. H. Efficient multicarbon formation in acidic CO_2 reduction via tandem electrocatalysis. *Nat. Nanotechnol.* **2024**, *19* (3), 311−318.
(36) Wu, Q.; Jiang, K.; Han, J.; Chen, D.; Luo, M.; Lan, J.; Peng, M.; Tan, Y. Dynamic shrinkage of metal-oxygen bonds in atomic Co-doped nanoporous RuO_2 for acidic oxygen evolution. *Science China Materials* **2022**, *65* (5), 1262−1268.
(37) Pan, S.; Li, H.; Liu, D.; Huang, R.; Pan, X.; Ren, D.; Li, J.; Shakouri, M.; Zhang, Q.; Wang, M.; Wei, C.; Mai, L.; Zhang, B.; Zhao, Y.; Wang, Z.; Graetzel, M.; Zhang, X. Efficient and stable noble-metal-free catalyst for acidic water oxidation. *Nat. Commun.* **2022**, *13* (1), 2294.
(38) Wang, X.; Zhong, H.; Xi, S.; Lee, W. S. V.; Xue, J. Understanding of Oxygen Redox in the Oxygen Evolution Reaction. *Adv. Mater.* **2022**, *34* (50), No. 2107956.
(39) Ping, X.; Liu, Y.; Zheng, L.; Song, Y.; Guo, L.; Chen, S.; Wei, Z. Locking the lattice oxygen in RuO_2 to stabilize highly active Ru sites in acidic water oxidation. *Nat. Commun.* **2024**, *15* (1), 2501.
(40) Miao, X.; Zhang, L.; Wu, L.; Hu, Z.; Shi, L.; Zhou, S. Quadruple perovskite ruthenate as a highly efficient catalyst for acidic water oxidation. *Nat. Commun.* **2019**, *10* (1), 3809.
(41) Zagalskaya, A.; Alexandrov, V. Role of Defects in the Interplay between Adsorbate Evolving and Lattice Oxygen Mechanisms of the Oxygen Evolution Reaction in RuO_2 and IrO_2. *ACS Catal.* **2020**, *10* (6), 3650−3657.
(42) Zhou, C.; Li, L.; Dong, Z.; Lv, F.; Guo, H.; Wang, K.; Li, M.; Qian, Z.; Ye, N.; Lin, Z.; Luo, M.; Guo, S. Pinning effect of lattice Pb suppressing lattice oxygen reactivity of Pb-RuO_2 enables stable industrial-level electrolysis. *Nat. Commun.* **2024**, *15* (1), 9774.

https://doi.org/10.1021/jacs.4c18238
J. Am. Chem. Soc. 2025, 147, 8720−8731